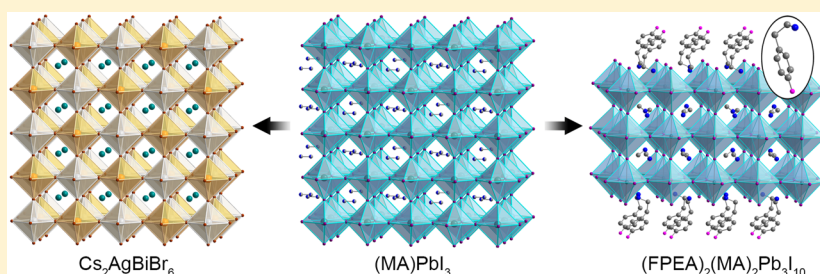# Chemical Approaches to Addressing the Instability and Toxicity of Lead−Halide Perovskite Absorbers

Adam H. Slavney, Rebecca W. Smaha, Ian C. Smith, Adam Jaffe, Daiki Umeyama, and Hemamala I. Karunadasa*

Department of Chemistry, Stanford University, Stanford, California 94305, United States

**S** *Supporting Information*



Cs₂AgBiBr₆          (MA)PbI₃          (FPEA)₂(MA)₂Pb₃I₁₀

**ABSTRACT:** The impressive rise in efficiencies of solar cells employing the three-dimensional (3D) lead−iodide perovskite absorbers $APbI_3$ (A = monovalent cation) has generated intense excitement. Although these perovskites have remarkable properties as solar-cell absorbers, their potential commercialization now requires a greater focus on the materials' inherent shortcomings and environmental impact. This creates a challenge and an opportunity for synthetic chemists to address these issues through the design of new materials. Synthetic chemistry offers powerful tools for manipulating the magnificent flexibility of the perovskite lattice to expand the number of functional analogues to $APbI_3$. To highlight improvements that should be targeted in new materials, here we discuss the intrinsic instability and toxicity of 3D lead−halide perovskites. We consider possible sources of these instabilities and propose methods to overcome them through synthetic design. We also discuss new materials developed for realizing the exceptional photophysical properties of lead−halide perovskites in more environmentally benign materials. In this Forum Article, we provide a brief overview of the field with a focus on our group's contributions to identifying and addressing problems inherent to 3D lead−halide perovskites.

## ■ INTRODUCTION

Since the first report of $(MA)PbI_3$ (MA = $CH_3NH_3^+$) as a solar-cell absorber in 2009,[1] research on lead−halide perovskites has greatly expanded in scale and scope. Lead−halide perovskites exhibit an unusual combination of photophysical and electronic properties important for solar-cell absorbers including strong band-edge absorption, long carrier-recombination lifetimes, ambipolar charge conduction, and a high tolerance for defects.[2] The ability to deposit high-quality halide perovskite films from solution further allows for inexpensive, large-scale device fabrication. The largest driver for research in this field has been the effort to improve power conversion efficiencies (PCEs) of perovskite solar cells. This intense activity has resulted in PCEs of perovskite solar cells increasing from the initial value of 4% to over 20% in only 6 years. Similar increases in PCEs for other absorber technologies have required several decades.[3]

This rapid increase in device efficiencies has been realized primarily through improvements in film deposition and device architecture. Although small changes to the material composition (e.g., mixed-halide perovskites or perovskites with different organic cations) have afforded improvements to device performance and stability, the perovskite absorbers used

in these devices have not been substantially altered. Because perovskite-based devices are now being considered for commercialization, greater attention must be directed toward problems intrinsic to lead−halide perovskites. The structural and electronic basis for the lead−halide perovskites' remarkable photophysical characteristics also remains to be fully understood. Identifying and synthesizing new functional analogues to these absorbers will help us to better understand overarching design rules for synthesizing broader classes of high-performing absorbers.

To highlight improvements that should be targeted in the next generation of absorbers, here we discuss the intrinsic instability of three-dimensional (3D) lead−halide perovskites to moisture, light, and heat. We present possible origins of these instabilities and propose methods to circumvent them through targeted material design. We also examine the lead perovskite's potential environmental impact and discuss less toxic materials developed toward addressing these concerns. Here, we briefly review the field with a focus on changes to the

composition, structure, and dimensionality of the bulk material. This overview excludes the considerable advances in film fabrication and encapsulation methods, which may kinetically suppress decomposition pathways. We also exclude from our discussion the role of extrinsic additives and surfactants, which can improve film coverage and crystallinity. As a Forum Article, we provide more detailed descriptions of our group's contributions to this field. In particular, the initial demonstration of (1) two-dimensional (2D) perovskites as solar-cell absorbers with greater moisture resistance,[4] (2) light-induced dynamics in mixed-halide perovskites[5] and their mitigation through material compression,[6] and (3) the promising photophysical properties of halide double perovskites, which can accommodate nontoxic and stable metals.[7]

# ■ RESULTS AND DISCUSSION

**1. Halide Perovskite Structure.** Perovskites of the form $A^IB^{II}X_3$ (X = halide) consist of anionic frameworks of corner-sharing B−X octahedra. To provide charge compensation, cations reside in the cavities defined by eight adjacent octahedra (the A site). Organic−inorganic hybrid perovskites, such as $(MA)PbI_3$ (Figure 1A),[8] have organic A-site cations. Note that
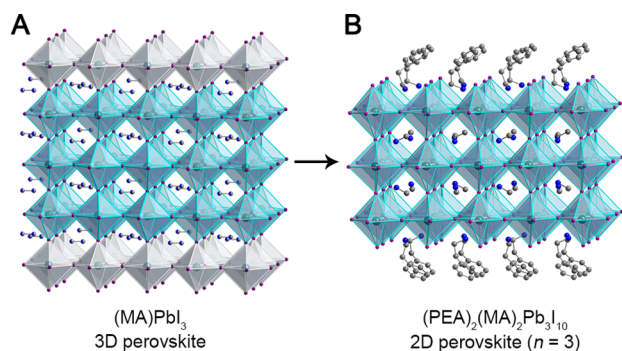


**Figure 1.** (A) Single-crystal XRD structures of $(MA)PbI_3$ (MA = $CH_3NH_3^+$)[6] and (B) $(PEA)_2(MA)_2Pb_3I_{10}$ (PEA = $C_6H_5(CH_2)_2NH_3^+$).[4] The inorganic layers in part B can be structurally derived from the 3D lattice by slicing along specific crystallographic planes (turquoise sheets in part A). Turquoise, purple, blue, and gray spheres represent Pb, I, N, and C atoms, respectively. The C and N atoms in $(MA)PbI_3$ are equally disordered. H and some disordered atoms are omitted for clarity. Reprinted with permission from ref 4. Copyright 2014 John Wiley and Sons.

these hybrid lead−halide perovskites are not organolead, organometallic, or organohalide compounds (although the terms have often been used) because they do not contain C−Pb or C−X bonds. Elemental composition and thermodynamic variables such as temperature and pressure dictate the perovskite lattice's symmetry (e.g., cubic, tetragonal, or orthorhombic). Here, small changes to the lattice symmetry can substantially change the materials' photophysical properties. These 3D perovskites are a subset of the broader and structurally diverse perovskite family. Lower-dimensional perovskite structures consist of corner-sharing metal−halide octahedra that are connected in 0, 1, or 2 dimensions.

**2. Moisture Instability.** Early reports on the moisture instability of $(MA)PbI_3$ mention its transformation to the high-bandgap yellow solid $PbI_2$.[9] The rate of this decomposition depends on film quality, with water likely entering the film through grain boundaries.[10] Because MA tends to be hygroscopic, we sought to replace it with a more hydrophobic

molecule. However, the A-site cavity in the 3D perovskite lattice severely restricts the size of the A cation. For example, assuming purely ionic interactions, the Goldschmidt tolerance factor analysis[11] predicts that only A-site cations with an effective radius of 1.6−2.6 Å will fit in the lead−iodide lattice, while a single C−N bond in an organic ammonium cation is 1.5 Å in length.[12] We therefore turned to 2D perovskites that are far more tunable and can accommodate a greater variety of organic cations.

**2.1. Layered Hybrid Perovskites with Enhanced Moisture Stability.** Layered or 2D perovskites consist of anionic metal−halide sheets partitioned by ordered arrays of organic cations (Figure 1B).[13] The most common 2D perovskites contain a single metal−halide sheet per inorganic layer and are designated as n = 1 structures (n = number of metal−halide sheets in each inorganic layer). The optical and electronic properties of n = 1 lead−iodide perovskites have been studied for decades.[14] These materials typically have relatively large bandgaps ($E_g$) of ca. 2.6−2.9 eV and unusually large Coulombic attraction between photogenerated electrons and holes (excitons).[15] The exciton binding energies ($E_b$) in these 2D perovskites are typically around 300 meV.[15] The spatial confinement of the 2D sheets increases the 2D perovskite's $E_b$ value relative to that of the 3D perovskite. The $E_b$ of the 2D material is further increased by the low dielectric constant of the organic layers, which provides poor shielding of the electrons and holes generated in the inorganic layers.[15] Such large $E_g$ and $E_b$ values allow for strong excitonic photoluminescence (PL), which has been used in light-emitting-diode,[16] green phosphor,[17] and white-light phosphor[18] applications. However, these $E_g$ and $E_b$ values are too high for typical solar-cell absorbers, where visible light should generate free carriers at room temperature.

To access a material that more closely resembles the 3D perovskite, we therefore considered 2D perovskites with higher values of n. A mixture of small and large organic cations leads to the assembly of 2D perovskites with thicker inorganic sheets.[19] We chose the $(PEA)_2(MA)_{n-1}Pb_nI_{3n+1}$ (PEA = $C_6H_5(CH_2)_2NH_3^+$) family of perovskites because they had notably low $E_b$ values, attributed to the higher dielectric constant of the polarizable aromatic groups compared to alkyl groups.[20] The n = 1 perovskite has reported $E_g$ and $E_b$ values of 2.57 eV and 220 meV, respectively.[14b,20] These values decrease for the n = 2 perovskite, which has $E_g$ and $E_b$ values of 2.32 eV and 170 meV, respectively.[14b,20] However, these values are still too high for efficient sunlight absorption and carrier separation in a standard solar cell. We therefore targeted the n = 3 perovskite to better mimic the properties of the 3D (n = ∞) perovskite. In order to access a well-defined material, we obtained the single-crystal X-ray diffraction (XRD) structure of $(PEA)_2(MA)_2Pb_3I_{10}$, the first crystallographically characterized n = 3 lead−iodide perovskite (Figure 1B). Using optical absorption spectroscopy, we estimated $E_g$ and $E_b$ values for $(PEA)_2(MA)_2Pb_3I_{10}$ as ca. 2.1 eV and ca. 40 meV, respectively.[4] This $E_g$ value is close to the ideal value (ca. 1.9 eV) for the higher bandgap absorber in a tandem solar cell.[21]

Solar cells constructed with the n = 3 perovskite showed an initial device efficiency of 4.73% and an open-circuit voltage of 1.18 V.[4] Importantly, these devices could be fabricated in humid air. Although these efficiencies were lower than those of cells with 3D perovskites, this work first showed that 2D perovskites can serve as solar-cell absorbers and that they provide distinct advantages:[4]

(1) Due to the hydrophobic nature of the organic layers, the 2D material is far more resistant to moisture compared to the 3D analogue (Figure 2A,B), leading to lower manufacturing costs and improved device lifetimes.
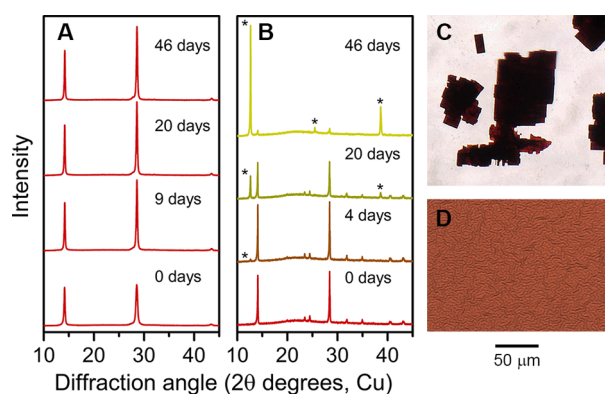


**Figure 2.** Powder XRD patterns of (A) $(PEA)_2(MA)_2Pb_3I_{10}$ films and (B) $(MA)PbI_3$ films upon exposure to 52% relative humidity. Asterisks denote reflections corresponding to $PbI_2$. (C) Micrograph of $(PEA)_2(MA)_2Pb_3I_{10}$ crystals. (D) Bright-field micrograph of a typical $(PEA)_2(MA)_2Pb_3I_{10}$ film on glass. Adapted from ref 4. Copyright 2014 Wiley-VCH Verlag GmbH & Co. KGaA.

(2) The layered structure affords high-coverage films using a single spin-coating step without annealing (Figure 2D).

(3) High cell voltages (that routinely exceed 1.1 V) can be easily accessed because of the material's higher-bandgap compared to $(MA)PbI_3$.

Subsequently, the analogous $n = 3$ perovskite $(CH_3(CH_2)_3NH_3)_2(MA)_2Pb_3I_{10}$ was used as an absorber in a solar cell with an initial device efficiency of 4.02% and an open-circuit voltage of 0.929 V.[22] The greatest advantage of the 2D material is the tunability of both the organic and inorganic layers. For example, we proposed that higher values of $n$, as single-phase materials or as mixtures, could afford higher device efficiencies as the inorganic components more closely resemble the 3D perovskite.[4] Recently, several groups have indeed

realized higher-efficiency 2D perovskite solar cells by increasing the ratio of small-to-large organic cations to form thicker inorganic layers.[23] Importantly, the organic components can be tuned independently of the inorganic layers. Hydrophobic molecules could further increase moisture stability, conductive molecules could facilitate charge transport, and molecular photosensitizers could expand the material's absorption cross section.

To further enhance the 2D material's stability, we report here the use of hydrophobic fluorinated molecules in the organic layers. We find that even the substitution of a single F atom in PEA can improve the material's moisture resistance (Figure 3D). The $n = 1$ perovskite $(FPEA)_2PbI_4$ (FPEA = 4-$FC_6H_4(CH_2)_2NH_3^+$; Figure 3A) has been previously reported,[24] and its photostability with respect to $(PEA)_2PbI_4$ has been evaluated.[25] We synthesized the $n = 2$ and 3 members of this family and obtained their single-crystal XRD structures (Figure 3B,C; details in the Supporting Information). Although moisture tolerance is related to film quality, we consistently find that the fluorinated perovskites are more moisture-stable than their nonfluorinated analogues when films of similar quality are compared. We therefore propose that incorporating heavily fluorinated groups into absorbers with high $n$ values should lead to still greater moisture resistance without compromising device performance.

Although we isolate single-phase crystals of the $n = 3$ perovskites through solution-state self-assembly, their films show absorption features indicating a small distribution of $n$ values.[4] This is likely because of the faster kinetics of film formation upon spin coating compared to the slower and reversible crystallization process in solution. At very high ratios of small-to-large cations, the large cations serve the role of additives that modify the surfaces and grain boundaries. For example, butylphosphonic acid ammonium additives have been reported to improve device performance and slow degradation of 3D perovskites.[26] Here, the organic additives are proposed to link adjacent grains in the film,[26] which is reminiscent of the organic layers in 2D perovskites.
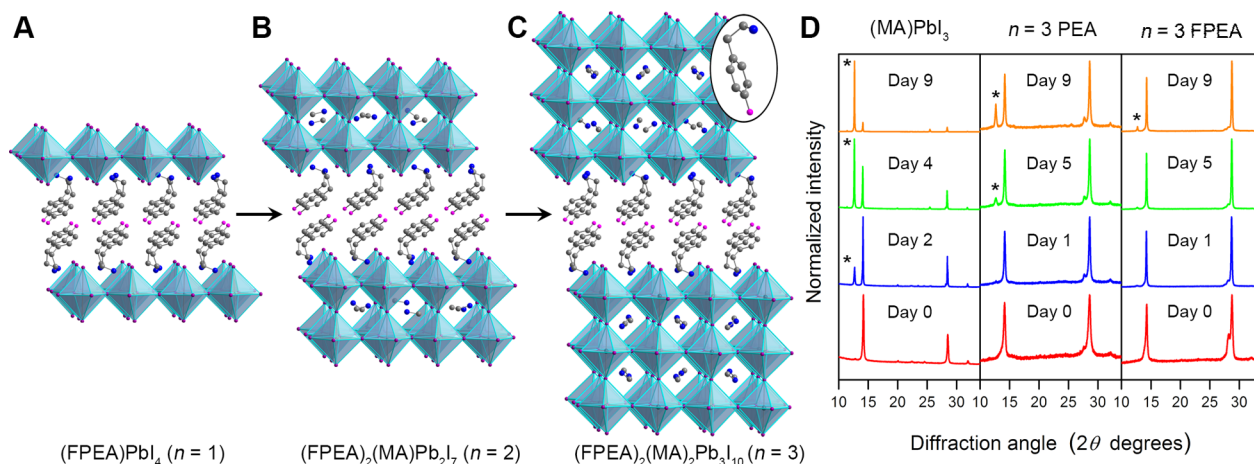


**Figure 3.** Single-crystal XRD structures of (A) $(FPEA)PbI_4$, (B) $(FPEA)_2(MA)Pb_2I_7$, and (C) $(FPEA)_2(MA)_2Pb_3I_{10}$ (FPEA = 4-$FC_6H_4(CH_2)_2NH_3^+$ (C inset) and MA = $CH_3NH_3^+$). Turquoise, purple, pink, blue, and gray spheres represent Pb, I, F, N, and C atoms, respectively. H and disordered atoms are omitted for clarity. As $n$ increases, the material's photophysical properties approach those of $(MA)PbI_3$ ($n = \infty$), while the organic layers provide moisture resistance. (D) Powder XRD patterns of $(MA)PbI_3$, $(PEA)_2(MA)_2Pb_3I_{10}$ ($n = 3$ PEA), and $(FPEA)_2(MA)_2Pb_3I_{10}$ ($n = 3$ FPEA) upon exposure to 66% relative humidity (PEA = $C_6H_5(CH_2)_2NH_3^+$). Asterisks correspond to reflections from $PbI_2$. The fluorinated perovskite appears to be the most moisture-resistant.

**2.2. Lead−Thiocyanide Hybrid Perovskites.** Another material proposed to improve on the moisture stability of $(MA)PbI_3$ is the Pb−I−SCN perovskite originally formulated as $(MA)[PbI(SCN)_2]$.[27] This material was attributed a similar bandgap to that of $(MA)PbI_3$ (1.5 eV) and similar performance as a solar-cell absorber, while showing improved moisture resistance.[27] However, a single-crystal XRD analysis of crystals obtained from the precursor solution to this material revealed the 2D perovskite $(MA)_2[PbI_2(SCN)_2]$ with terminal thiocyanides and bridging iodides (Figure 4A).[28] Although this 2D
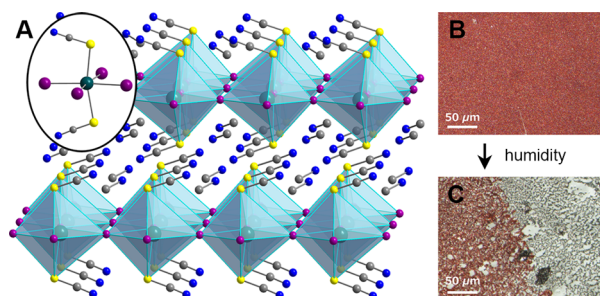


**Figure 4.** (A) Single-crystal XRD structure of $(MA)_2[PbI_2(SCN)_2]$.[28] Turquoise, purple, yellow, blue, and gray spheres represent Pb, I, S, N, and C atoms, respectively. H atoms are omitted. A $(MA)_2[PbI_2(SCN)_2]$ film before (B) and after (C) humidity exposure. Reproduced from ref 31. Copyright 2016 American Chemical Society.

perovskite has been attributed a low bandgap (1.5−1.6 eV),[28,29] it was recently shown to have a much higher bandgap (>2 eV) and confined charge carriers in the inorganic layers, consistent with its 2D structure.[30] In our hands, we found this 2D perovskite to be very sensitive to both ambient humidity and moderate (50 °C) heating in dry air. Analysis of the decomposition product (Figure 4B,C) using powder XRD and vibrational, optical absorption, and PL spectroscopy showed indications of $(MA)PbI_3$ formation.[31] This decomposition product can explain the low bandgap and promising properties as an absorber previously attributed to the 2D Pb−I−SCN perovskite. Because the devices were fabricated in humid air and with high-temperature annealing steps, the final composition of high-performing Pb−I−SCN perovskite absorbers is therefore uncertain. Residual $SCN^-$ may improve films containing primarily crystalline $(MA)PbI_3$ by passivating grain boundaries and/or improving film morphology. Several reports have claimed that substituting a small amount of $SCN^-$ into $(MA)PbI_3$ to access materials formulated as $(MA)[PbI_{3-x}(SCN)_x]$ leads to improved PL intensity[32] and device performance.[32a]

Although $(MA)_2[PbI_2(SCN)_2]$ has a much greater electronic confinement compared to $(MA)PbI_3$,[30] $SCN^-$ coordination brings interesting new properties. The material has low exciton binding energy (200 meV) compared to that of typical 2D lead−iodide perovskites (ca. 300 meV).[31] It further displays an unusually large pressure response, transitioning from translucent red to opaque black at 2.6 GPa, indicating a large reduction in bandgap.[31] Similar bandgap reductions occur at much higher pressures for 2D Cu−Cl perovskites (at 12 GPa)[33] and 2D Pb−I perovskites (at 24 GPa).[34] Therefore, relatively modest pressures can substantially change the bandgap and optical properties of $(MA)_2[PbI_2(SCN)_2]$, enabling new functionality.

## 3. Light Instability. 3.1. Mixed-Halide Perovskites. The valence-band maximum (VBM) of lead−halide perovskites has predominantly halide p-orbital character (mixed with lead s-orbital character), while the conduction-band minimum (CBM) is primarily formed from empty lead 6p orbitals.[35] Therefore, partial substitution of more electronegative halides for iodides in the perovskite lattice leads to a systematic bandgap increase as the valence band is lowered in energy. Such mixed-halide perovskites afford the higher bandgaps required for tandem solar cells that can achieve higher efficiencies compared to single-absorber devices.[36] However, achieving high voltages from devices employing mixed-halide perovskite absorbers has not been straightforward,[9,37] and the bromide-rich alloys have not yielded the high voltages expected from their bandgaps.

We recently reported on white-light emission from 2D perovskites, which we attributed to transient light-induced defects caused by self-trapped carriers.[18] Light-induced structural changes have also been reported in lead halides,[38] which have VBM and CBM compositions similar to those of the 2D and 3D lead−halide perovskites. We find that light-induced dynamics also occur in the mixed-halide perovskites $(MA)Pb(Br_xI_{1-x})_3$ (0.2 < $x$ < 1), which can explain the lower voltages obtained from devices with bromide-rich absorbers.[5]

The initial PL energies of $(MA)Pb(Br_xI_{1-x})_3$ (0 < $x$ < 1) films correspond to their bandgaps, with higher-bandgap materials affording higher-energy PL. However, upon light soaking for less than 1 min, the PL energy for 0.2 < $x$ < 1 perovskites discretely redshifts to ca. 1.7 eV (Figure 5A).
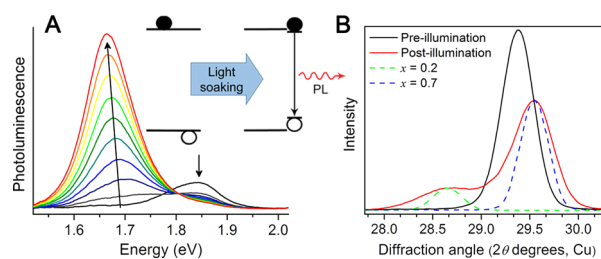


**Figure 5.** (A) Thin-film PL spectra of the $x = 0.4$ member of the $(MA)Pb(Br_xI_{1-x})_3$ family over 45 s under 457 nm light. Inset: Schematic showing light-induced trap formation in perovskites (filled circle = electron; empty circle = hole). (B) The (200) XRD peak of an $x = 0.6$ film before (black) and after (red) white-light soaking for 5 min. Dotted lines show the expected peak positions for $x = 0.2$ (green) and $x = 0.7$ (blue) films. Reproduced with permission from ref 5. Copyright 2015 Royal Society of Chemistry.

Notably, these changes are reversible, and the initial PL spectra are regained after the materials are allowed to equilibrate in the dark for 5 min. Characterization of the illuminated material reveals transient light-induced changes. Sub-bandgap absorption states that appear only upon material illumination indicate the reversible formation of trap states. Furthermore, the sharp reflections in the powder XRD patterns of the perovskite films split into two sets of reflections upon visible-light soaking, suggesting phase segregation to a larger and a smaller lattice (Figure 5B). The temperature dependence of the low-energy PL band's initial growth rate allows us to calculate the activation energy for this process as 0.27(6) eV. This value compares well with activation energies for halide mobility in related metal halides.[39] Compiling this evidence, we proposed that light induces the segregation of mixed-halide alloys into

iodide- and bromide-rich domains. Due to the greater electronegativity of bromine, the VBM of the iodide-rich domains is higher in energy than the VBM of bromide-rich domains. Holes are therefore better stabilized in iodide-rich domains, which may drive halide segregation. Entropy and local lattice strain could drive the material back to a homogeneous alloy in the dark.[5] The calculated phase diagram of the mixed-halide perovskites indicates phases that are unstable as homogeneous alloys, which may contribute to halide segregation.[40] Sub-bandgap features in mixed-halide perovskites with high bromine content also suggest phase segregation in some as-deposited films.[41]

*3.2. Mitigating the PL Redshift in Mixed-Halide Perovskites.* Light-induced formation of low-energy trap states has now been observed in several $APb(Br_xI_{1-x})_3$ perovskites (A = MA,[5] $[(NH_2)_2CH]^+$,[5,42] $Cs^+$ [43]) and may limit obtainable voltages from these absorbers. Recent work has shown that this PL redshift is mitigated in high-quality films.[44] Ion migration can be faster at grain boundaries than through the bulk material,[45] which could account for this effect. This redshift is also reported to be reduced in hybrid perovskites with mixed A-site cations[46] and in inorganic perovskites,[43] suggesting that material design can influence these light-induced dynamics. Because our proposal of halide segregation under illumination requires halide mobility, we reasoned that compressing the lattice should change the kinetics and/or thermodynamics of halide migration. We therefore applied hydrostatic pressure to $(MA)Pb(Br_xI_{1-x})_3$ $(0 < x < 1)$ using diamond-anvil cells and monitored their PL evolution as a function of illumination time and pressure.[6]

*3.3. Effects of Lattice Compression.* The perovskites $(MA)PbX_3$ $(X = I^-$ or $Br^-)$ transition from a low-pressure $\alpha$ phase to a high-pressure $\beta$ phase upon compression (Figure 6).[6,47] Using Glazer notation for describing octahedral rotations
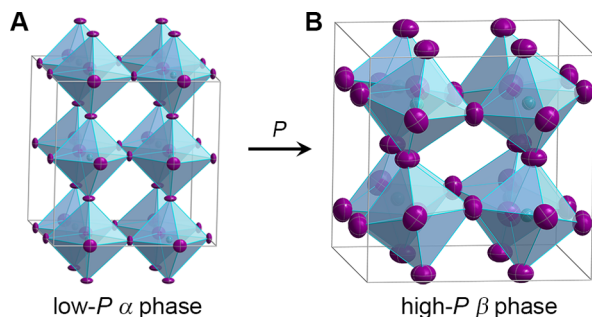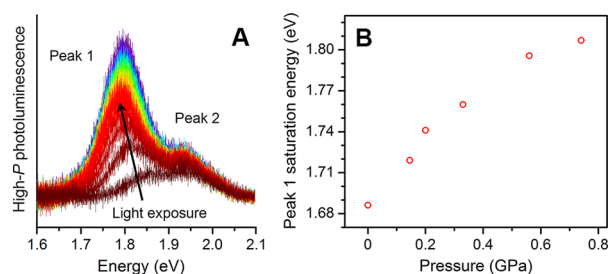


**Figure 7.** A) PL evolution with light soaking over 8 s intervals for a powder of the $x = 0.6$ member of the $(MA)Pb(Br_xI_{1-x})_3$ (MA = $CH_3NH_3^+$) family at 0.6 GPa. B) Pressure dependence of the energy to which peak 1 asymptotes with light exposure. Figure reproduced from ref 6.

dominates the PL response at still higher pressures. In contrast to peak 1, peak 2's energy is invariant with illumination time. The pressure evolution of peak 2's energy suggests that the emission arises from the parent mixed-halide material, where halide segregation is suppressed through lattice compression. Although application of very high pressures may not be practical for most technologies, the effects of mechanical pressure can be simulated chemically. For example, introducing ions that are mismatched in size with the lattice can exert steric pressure. Theoretical studies have shown a correlation between pressure effects mediated through mechanical and steric compression.[49] Therefore, ion substitution provides additional means of tuning the material's photophysical properties through chemical pressure and has already shown some success.[46,50]

**4. Thermal Instability.** The hybrid perovskites $(MA)PbX_3$ $(X = Br^-$ or $I^-)$ are not stable to heating in air or dry $N_2$. Although thermogravimetric analyses obtained at relatively fast scan rates suggest material stability, extended heating even at moderate temperatures of 60 °C[7] or 85 °C[51] leads to a loss of $CH_3NH_2$ and HX, leaving solid $PbX_2$. Loss of volatile products can drive the following equilibrium to the right according to Le Châtelier's principle:

$$CH_3NH_3I(s) \leftrightarrow CH_3NH_2(g) + HI(g)$$

Perovskites containing formamidinium in the A site are more stable to heat,[52] which is consistent with the amine's higher basicity. Therefore, we postulate that still more basic cations should lead to greater heat resistance. Material encapsulation will likely reduce this decomposition pathway by preventing loss of volatile small molecules. Maintaining an atmosphere of $CH_3NH_2 \cdot HI$ when annealing perovskite films at high temperatures can also prevent thermal degradation.[53] However, inherent thermal stability would be an advantage for typical solar cells that reach temperatures of 50−70 °C during routine operation[54] and still higher temperatures during device fabrication. Substituting MA with inorganic A-site cations greatly increases the material's thermal stability. For example, $CsPbBr_3$[55] is more thermally stable than $(MA)PbBr_3$.[56] The inorganic iodide analogue $CsPbI_3$ forms a yellow one-dimensional (1D) structure at room temperature and is thermodynamically stable as a 3D perovskite only at temperatures above 330 °C.[57] There are, however, reports of kinetically trapping the metastable 3D perovskite phase,[58] as well as using a mixture of inorganic and organic A-site cations to improve thermal stability.[46,50]
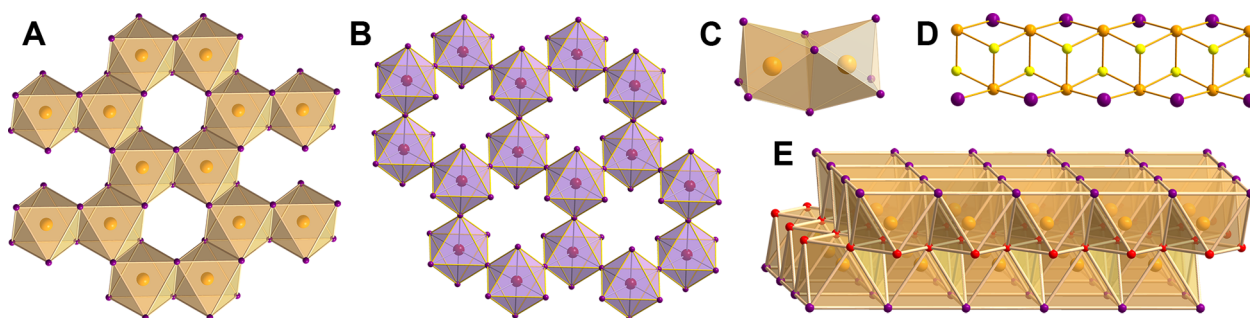


**Figure 6.** Single-crystal XRD structures of $(MA)PbI_3$ at A) ambient pressure ($\alpha$ phase; $Fmmm$) and B) at 0.7 GPa ($\beta$ phase; $Im\bar{3}$). Turquoise and purple ellipsoids represent Pb and I atoms, respectively. Disordered iodides and MA cations are omitted for clarity. Figure reproduced from ref 6.

in perovskites,[48] this constitutes a transition from $a^0a^0c^-$ to $a^+a^+a^+$ for the iodide perovskite and a transition from $a^0a^0a^0$ to $a^+a^+a^+$ for the bromide perovskite. In their $\beta$ phases, the iodide, bromide, and mixed-halide perovskites adopt the same cubic space group: $Im\bar{3}$. The PL redshift seen at ambient pressure in $(MA)Pb(Br_{0.6}I_{0.4})_3$ is also evident at higher pressures (Figure 7A, peak 1). However, higher-energy steady-state PL is attained at higher pressure (Figure 7B). This suggests that application of less than 1 GPa can increase obtainable voltages from these absorbers. Furthermore, a new PL band emerges at pressures close to the $\alpha-\beta$ transition (Figure 7A, peak 2), which

**Figure 8.** Fragments of the inorganic lattices in (A) 2D BiI$_3$,[74] (B) 2D Cs$_3$Sb$_2$I$_9$,[73] (C) 0D Cs$_3$Bi$_2$I$_9$,[71,72] (D) 1D BiSI,[70] and (E) 2D BiOI,[69] which have been evaluated as nontoxic solar-cell absorbers. Orange, dark-red, purple, yellow, and red spheres represent Bi, Sb, I, S, and O atoms, respectively.

**5. Toxicity of Lead–Halide Perovskites.** The toxicity of Pb$^{2+}$ is a primary concern for the wide-scale implementation of halide-perovskite absorbers. Lead is a potent human and environmental toxin. Even low exposure levels have been associated with significant health problems including nerve damage, renal failure, and impaired brain development.[59] Lead's toxicity primarily arises from its ability to inhibit key antioxidant enzymes, such as glutathione reductase, by forming covalent attachments to the active-site thiol groups.[60] The neurological effects of lead poisoning arise from its ability to replace Ca$^{2+}$ in various signaling proteins (e.g., protein kinase C), interfering with signal transduction throughout the central nervous system.[61] A recent study assessing the potential risks of lead contamination over the lifecycle of a hypothetical perovskite solar module concluded that their commercialization would require a fail-safe encapsulation method that would contain toxic species even in the event of a catastrophic accident.[62] Significant effort would also be required during the manufacturing and decommissioning phase of the module lifecycle to ensure worker safety and prevent environmental contamination.[62] These safety concerns are more acute for the lead perovskites than for older technologies such as CdTe largely because PbI$_2$ is water-soluble (the $K_{sp}$ value for PbI$_2$ at 25 °C is $9.8 \times 10^{-9}$,[63] amounting to ca. 620 mg of PbI$_2$ in 1 L of water) and therefore environmentally mobile, which prevents easy containment and cleanup in the event of accidental release. This problem is likely common to all materials containing toxic elements that can be deposited from solution because high solubility, particularly in polar solvents, enables easy extraction of the material into the environment by water. Therefore, identifying less toxic materials that mimic the optoelectronic properties of the lead–halide perovskites would constitute a major advance in this field.

*5.1. 3D Tin–Halide Perovskites.* Both tin[64] and germanium[65] form 3D halide perovskites. The Sn$^{2+}$ perovskites have been studied as potentially less toxic analogues of the lead-based perovskite absorbers, and the efficiencies of devices employing these materials have reached ca. 6%.[66] However, both tin and germanium perovskites are susceptible to oxidation to form Sn$^{4+}$ and Ge$^{4+}$. In contrast to the lead perovskites, the VBMs of these materials have significant metal s-orbital character, leading to the metal's facile oxidation, resulting in uncontrolled doping and rapid decomposition. The greater relativistic contraction[67] of the lead 6s orbital likely places it lower in the valence band and protects it from oxidation.

*5.2. Zero-Dimensional (0D), 1D, and 2D Metal Halides.* Bismuth (Bi$^{3+}$) has historically been used as a nontoxic

replacement for lead (Pb$^{2+}$) in diverse applications in chemistry and materials science.[68] The 2D solids BiOI[69] and BiSI[70] have been previously considered for photovoltaic applications. More recently, several other bismuth-containing materials have been investigated as possible replacements for (MA)PbI$_3$ (Figure 8). However, likely because of the increased charge of Bi$^{3+}$ compared to Pb$^{2+}$, most of these compounds crystallize as low-dimensional structures. The 0D dimers A$_3$Bi$_2$I$_9$ (A = MA or Cs$^+$)[71] have been evaluated as absorbers.[72] Replacing Cs$^+$ or MA with the smaller Rb$^+$ cation gives a 2D derivative of the perovskite structure Rb$_3$Bi$_2$I$_9$ and changes the bandgap transition from indirect to direct.[72a] The Sb$^{3+}$ analogue Cs$_3$Sb$_2$I$_9$ has also been explored and, depending on the synthetic conditions, crystallizes as a dimer or a layered phase, which is isostructural with 0D Cs$_3$Bi$_2$I$_9$ or 2D Rb$_3$Bi$_2$I$_9$, respectively.[73] The 2D solid BiI$_3$[74] and the 2D perovskite (MA)$_2$CuBr$_{4-x}$Cl$_x$[75] have also been examined as absorbers.

Given the importance of device optimization for achieving high PCEs, the low initial efficiencies of devices (Table 1) using

**Table 1. Selected Parameters for Lead-Free Low-Dimensional Metal Halides Evaluated as Absorbers**

| compound | dimensionality | $E_g$ (eV)[a] | initial PCE % |
|---|---|---|---|
| (MA)$_3$Bi$_2$I$_9$[72b,c] | 0D | 2.0 (ind.) | 0.12[72b] |
| Cs$_3$Bi$_2$I$_9$[72a,b] | 0D | 1.9 (ind.) | 1.09[72b] |
| Cs$_3$Sb$_2$I$_9$[73] | 0D | 2.4 (ind., calcd) | n/a |
| BiSI[70] | 1D | 1.6 (ind.) | 0.25[70b] |
| Cs$_3$Sb$_2$I$_9$[73] | 2D | 2.0 | <1 |
| Rb$_3$Bi$_2$I$_9$[72a] | 2D | 2.1 | n/a |
| BiI$_3$[74] | 2D | 1.8 (ind.) | 0.3[74a] |
| BiOI[69] | 2D | 1.8 (ind.) | 0.1[69b] |
| (MA)$_2$CuBr$_{4-x}$Cl$_x$[75] | 2D | 2.9–3.1 | ~0.02 |

[a]ind. = indirect. calcd = calculated.

the materials discussed above should not be viewed negatively. However, lower-dimensional materials often have strong confinement effects, which are less desirable for typical photovoltaic devices. Carrier effective masses typically increase with decreasing dimensionality, leading to poor transport along particular lattice directions that can impede carrier extraction.[73,75] Furthermore, quantum confinement effects[76] greatly increase the exciton binding energy in low-dimensional materials. Materials with strongly bound excitons require different cell architectures, such as bulk heterojunctions, to generate appreciable photocurrent because the neutral exciton is unaffected by the electric field used to separate carriers in conventional solar cells.[77] As in the $n$ = 3 perovskites, thicker
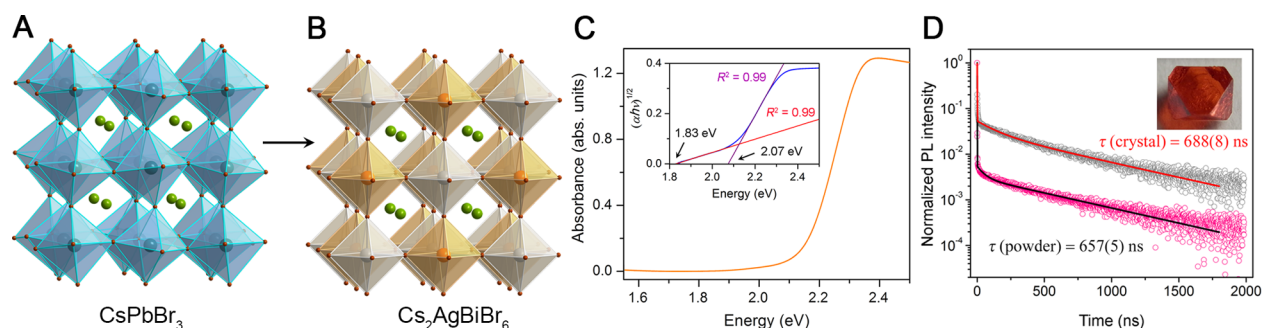
**Figure 9.** Single-crystal XRD structures of (A) CsPbBr$_3$[55] and (B) Cs$_2$AgBiBr$_6$.[7] Turquoise, orange, white, brown, and green spheres denote Pb, Bi, Ag, Br, and Cs atoms, respectively. (C) Absorption spectrum of Cs$_2$AgBiBr$_6$. Inset: Tauc plot of the absorption data showing the two linear regions characteristic of an indirect bandgap. (D) Time-resolved room-temperature PL and fits for the PL decay time ($\tau$) in powder (pink/black) and single-crystal (gray/red) samples. Inset: Photograph of a Cs$_2$AgBiBr$_6$ single crystal. Parts C and D are reproduced from ref 7. Copyright 2016 American Chemical Society.

inorganic structures can decrease these confinement effects and afford more efficient carrier extraction in a solar cell.[4] However, to eliminate confinement effects entirely, we sought a 3D material to capture the photophysical properties of APbI$_3$.

The Pb$^{2+}$ orbitals play a critical role in the band edges of the lead perovskites[35] and are believed to be partially responsible for the high defect tolerance and strong absorption observed in (MA)PbI$_3$ and related compounds.[78] Therefore, the most straightforward method of emulating the electronic structure of lead−halide perovskites is to incorporate metals with the same electronic configuration as Pb$^{2+}$. Both Tl$^+$ and Bi$^{3+}$ have the same electronic configuration as Pb$^{2+}$. Because thallium is more toxic than lead, we first focused our efforts on incorporating bismuth into a 3D perovskite lattice.

*5.3. 3D Bismuth−Halide Double Perovskites.* A principle challenge to replacing Pb$^{2+}$ with Bi$^{3+}$ in a 3D lattice is to accommodate the difference in charge. Perovskites of the form A$^I$B$^{II}$X$_3$ (X = halide) require a divalent B-site cation. To incorporate Bi$^{3+}$ into the 3D perovskite lattice, we therefore moved to the expanded double-perovskite lattice A$^I_2$BB′X$_6$. Although the B and B′ sites must still provide a combined charge of 4+, the charge can be divided equally or unequally. Oxide double perovskites (A$_2$BB′O$_6$) have been extensively studied over the past several decades and have proven to be an extremely versatile framework that can accommodate oxidation states from 1+ to 7+ in the B and B′ sites.[79] Halide double perovskites can accommodate metals with oxidation states of 2+/2+ and 1+/3+ in the B/B′ sites. Tetravalent cations could also be incorporated to form a 4+/0 perovskite, where the B′ site is vacant. The compound Cs$_2$Sn$^{IV}$I$_6$ adopts this structure[80] and has recently been explored as a photovoltaic absorber[81] and hole conductor.[82] A wide variety of halide double perovskites (also called elpasolites) have been reported, mostly with combinations of monovalent alkali cations and trivalent lanthanide cations in the B site.[83] Other trivalent metals, including Cr$^{3+}$ and Fe$^{3+}$, have also been paired with alkali cations to form double perovskites.[84] Alternatively, Ag$^+$, Au$^+$, or Tl$^+$ can be used instead of the alkali cation as in Cs$_2$Au$^I$Au$^{III}$X$_6$ (X = Cl$^−$, Br$^−$, or I$^−$),[85] Cs$_2$Ag$^I$Au$^{III}$Cl$_6$,[86] or Cs$_2$Tl$^I$Tl$^{III}$Cl$_6$.[87] The vast majority of these compounds are chloride perovskites, with bromide and iodide analogues being far scarcer.

Prior to our work, we are aware of only one bismuth−halide double perovskite that has been well characterized: Cs$_2$NaBiCl$_6$.[88] The double perovskites Cs$_2$MBiCl$_6$ (M = Li$^+$, K$^+$, Rb$^+$, or Tl$^+$) have also been reported.[89] Because these compounds were all chlorides and reported to be colorless

solids, we focused on synthesizing compounds with heavier halides, which should afford smaller bandgaps. By using Ag$^+$ as the B-site cation, we synthesized the double perovskite Cs$_2$AgBiBr$_6$ (Figure 9B).[7] The double perovskites Cs$_2$AgBiX$_6$ (X = Cl$^−$ or Br$^−$) were independently reported in a concurrent publication.[90] This was followed by a second report on Cs$_2$AgBiCl$_6$,[91] and subsequently the double perovskite (MA)$_2$KBiCl$_6$ was synthesized.[92]

The structure of Cs$_2$AgBiBr$_6$ (Figure 9B) is typical of ordered double perovskites consisting of silver- and bismuth-centered octahedra alternating in all three dimensions. This arrangement results in a doubled unit cell, compared to the simple perovskite, and a symmetry change from primitive to face-centered cubic. Our optical studies show that Cs$_2$AgBiBr$_6$ has an indirect bandgap of 1.95 eV (Figure 9C). This is within the required bandgap range for the top absorber in a tandem solar cell paired with a silicon bottom absorber.[21]

The lead perovskites show remarkably long carrier recombination lifetimes for direct-bandgap semiconductors (up to 1 $\mu$s for (MA)PbI$_3$ and up to 350 ns for (MA)PbBr$_3$),[2a] which are a critical component of their superior performance. Indirect-bandgap materials should have longer lifetimes compared to direct-bandgap materials. However, thus far, indirect-bandgap bismuth halides evaluated as absorbers have shown short lifetimes ranging from ca. 1[74b] to 6 ns.[72c] Time-resolved PL decay curves of Cs$_2$AgBiBr$_6$ show a rapid decay occurring with a characteristic time of a few nanoseconds followed by a much longer-lived tail with a characteristic time of ca. 660 ns (Figure 9D). Similar decay profiles have been observed in (MA)PbBr$_3$ single crystals and films and (MA)PbI$_3$ single crystals, and the initial rapid PL decay has been attributed to carrier recombination at surface sites.[2a] Due to its indirect bandgap, light is not as efficiently absorbed at the bandgap onset in Cs$_2$AgBiBr$_6$ compared to direct-bandgap absorbers such as (MA)PbI$_3$. Therefore, a thicker absorber layer is required in a device, which increases carrier recombination probability prior to charge extraction. Although further studies are required to conclusively assign the origins of the PL decay processes, the long-lived recombination process in Cs$_2$AgBiBr$_6$ is promising for photovoltaic applications. It suggests that carriers could reach the current collectors prior to recombination, especially if a thicker absorber layer is required. Notably, similar lifetimes are obtained for this long-lived process in both single crystals and powders, suggesting that films of the material would also display a long carrier recombination lifetime. Because of the material's indirect bandgap and low photo-

luminescence quantum efficiency, both the fast and slow decays observed here are likely related to nonradiative trap-assisted decay (Shockley−Read−Hall recombination). This suggests that the decay processes may not be inherent to $Cs_2AgBiBr_6$ and could potentially be extended or eliminated by employing surface treatments, higher-purity precursors, and/or optimized synthetic conditions. Minority-carrier lifetimes in silicon, the most well-explored indirect-bandgap material, have been shown to vary from nanoseconds to milliseconds depending on material treatment.[93] Further investigations of the behavior of excited carriers in $Cs_2AgBiBr_6$ are ongoing.

Preliminary stability studies show that $Cs_2AgBiBr_6$ is stable to heating at 100 °C for 3 days in air and to a 30-day air exposure at 55% relative humidity. The lack of volatile small molecules (e.g., $CH_3NH_2$, HX) likely enhances the material's thermal stability with respect to $(MA)PbX_3$ (X = $Br^-$ or $I^-$). Exposing $Cs_2AgBiBr_6$ to a broad-spectrum halogen lamp at 0.75 suns for 30 days under $N_2$ at 50 °C led to no decomposition detectable by powder XRD. However, after 15 days of light exposure, we noticed some surface discoloration. Because silver halides can be light-sensitive,[94] replacing $Ag^+$ with another monovalent cation could further improve the material's photostability. A separate report showed that when $Cs_2AgBiBr_6$ was exposed to light, air, and moisture over 30 days, the material deteriorated more rapidly.[90]

The $A^IB^{II}X_3$ (X = halide) perovskite lattice has so far restricted substitution of lead to divalent metals. Our work expands the field of perovskite solar-cell research to $A^I_2BB'X_6$ double perovskites, which can accept a greater variation of B- and B′-site metal oxidation states. Furthermore, as with $ABX_3$ perovskites, both inorganic and organic cations can be substituted at the A site and the halides can be varied or mixed. Therefore, double perovskites provide a more accommodating platform for synthesizing functional analogues to the lead−halide perovskites with nontoxic and stable metals.

## ■ EXPERIMENTAL SECTION

The perovskites $(FPEA)_2(MA)_{n-1}Pb_nI_{3n+1}$ (FPEA = 4-$FC_6H_4(CH_2)_2NH_3^+$; MA = $CH_3NH_3^+$; n = 1, 2, and 3) were synthesized by combining stoichiometric ratios of (FPEA)I, (MA)I, and $PbI_2$ in acetone/nitromethane or acetonitrile/nitromethane mixtures. Solid NaI was added to the solution to enhance the solubility of the lead salt. Slow solvent evaporation over 5−6 days afforded crystals suitable for X-ray structure determination. Detailed synthetic procedures, film deposition methods, and crystallographic data for the perovskites are available in the Supporting Information.

The CIFs for $(FPEA)_2PbI_4$, $(FPEA)_2(MA)Pb_2I_7$, $(FPEA)_2(MA)_2Pb_3I_{10}$ (100 K), and $(FPEA)_2(MA)_2Pb_3I_{10}$ (298 K) are given in the Supporting Information and have also been deposited in the Cambridge Crystallographic Data Center as CCDC 1488195, 1483085, 1483086, and 1483087, respectively.

## ■ CONCLUSIONS

We have presented several chemical strategies to potentially address some of the major obstacles to commercialization of perovskite-based solar cells. The increased attention on the instabilities and toxicity of $(MA)PbI_3$ has recently led to critical studies on the material's response to device manufacturing and operating conditions.[95]

With respect to our group's contributions to these efforts, we introduced 2D perovskites as absorbers with enhanced moisture tolerance, diagnosed light-induced dynamics in mixed-halide perovskites that led to lower device voltages and showed methods to mitigate this effect, and identified halide double perovskites as a large family of materials that could afford nontoxic materials with promising photophysical properties as solar-cell absorbers.

The $ABX_3$ perovskite lattice severely restricts the size of the A-site cation. Layered or 2D perovskites with thick inorganic sheets afford more moisture-resistant solar-cell absorbers owing to the hydrophobicity of the larger organic ammonium cations.[4] As the inorganic layers in 2D perovskites get thicker, these materials have the potential to closely match the absorption and transport properties of bulk $(MA)PbI_3$, while molecular-level hydrophobicity is imparted throughout the material as well as at surfaces and grain boundaries. The organic layers in 2D perovskites can be modified by a wide variety of organic molecules to impart additional functionality. For example, here we show that fluorinating the organic layers further enhances the material's moisture resistance. We also proposed that light-induced trap formation in mixed-halide perovskite absorbers occurs through halide segregation[5] and showed how mechanical compression can suppress this effect, potentially allowing for higher open-circuit voltages in devices employing these materials.[6] This strategy of applying pressure may also suppress hysteresis in all-iodide perovskite cells because halide mobility has been implicated in that process as well.[96] This motivates the use of chemical pressure and lattice strain to mimic the effects of mechanical pressure. Finally, to address the critical issue of lead toxicity, we synthesized the bismuth double perovskite $Cs_2AgBiBr_6$ and showed that this large family of materials should be further studied for optoelectronic applications.[7] The $A_2BB'X_6$ double perovskites greatly increase the diversity of cations that can occupy the B/B′ sites in the perovskite lattice and permit far greater modification and control of the electronic structure than was available with $ABX_3$ perovskites. We believe the following targets will further expand the technological reach of halide perovskites: (1) identification of new double perovskites with direct bandgaps, smaller bandgaps, or both; (2) controlled syntheses of layered perovskites where the organic and inorganic layers can be independently optimized to yield new functionality; (3) using mechanical or chemical pressure to realize new photophysical properties in these compressible solids.

In the past year alone, the composition of absorbers in the highest-performing perovskite devices has shifted away from the original $(MA)PbI_3$ as its limitations have become more apparent. It is likely that the formulation that will successfully compete with silicon is yet to be found but is also not too far distant. We believe that the future of perovskite photovoltaics is certainly bright and that new materials will help this technology achieve maturity.

## ■ ASSOCIATED CONTENT

**ⓢ Supporting Information**

The Supporting Information is available free of charge on the ACS Publications website at DOI: 10.1021/acs.inorg-chem.6b01336.

Experimental details and crystallographic data (PDF)

CIF for $(FPEA)_2PbI_4$ (CIF)

CIF for $(FPEA)_2(MA)Pb_2I_7$ (CIF)

CIF for $(FPEA)_2(MA)_2Pb_3I_{10}$ (100 K) (CIF)

CIF for $(FPEA)_2(MA)_2Pb_3I_{10}$ (298 K) (CIF)

## AUTHOR INFORMATION

**Corresponding Author**

*E-mail: hemamala@stanford.edu.

**Notes**

The authors declare no competing financial interest.

## REFERENCES

(1) Kojima, A.; Teshima, K.; Shirai, Y.; Miyasaka, T. *J. Am. Chem. Soc.* **2009**, *131*, 6050.

(2) (a) Shi, D.; Adinolfi, V.; Comin, R.; Yuan, M.; Alarousu, E.; Buin, A.; Chen, Y.; Hoogland, S.; Rothenberger, A.; Katsiev, K.; et al. *Science* **2015**, *347*, 519. (b) Green, M. A.; Ho-Baillie, A.; Snaith, H. J. *Nat. Photonics* **2014**, *8*, 506.

(3) NREL efficiency chart. This plot is courtesy of the National Renewable Energy Laboratory, Golden, CO; http://www.nrel.gov/ncpv/images/efficiency_chart.jpg.

(4) Smith, I. C.; Hoke, E. T.; Solis-Ibarra, D.; McGehee, M. D.; Karunadasa, H. I. *Angew. Chem., Int. Ed.* **2014**, *53*, 11232.

(5) Hoke, E. T.; Slotcavage, D. J.; Dohner, E. R.; Bowring, A. R.; Karunadasa, H. I.; McGehee, M. D. *Chem. Sci.* **2015**, *6*, 613.

(6) Jaffe, A.; Lin, Y.; Beavers, C. M.; Voss, J.; Mao, W. L.; Karunadasa, H. I. *ACS Cent. Sci.* **2016**, *2*, 201.

(7) Slavney, A. H.; Hu, T.; Lindenberg, A. M.; Karunadasa, H. I. *J. Am. Chem. Soc.* **2016**, *138*, 2138.

(8) Weber, D. *Z. Naturforsch.* **1978**, *33b*, 1443.

(9) Noh, J. H.; Im, S. H.; Heo, J. H.; Mandal, T. N.; Seok, S. I. *Nano Lett.* **2013**, *13*, 1764.

(10) Grancini, G.; D'Innocenzo, V.; Dohner, E. R.; Martino, N.; Mosconi, E.; Srimath Kandada, A. R.; De Angelis, F.; Karunadasa, H. I.; Hoke, E. T.; Petrozza, A. *Chem. Sci.* **2015**, *6*, 7305.

(11) Goldschmidt, V. M. *Naturwissenschaften* **1926**, *14*, 477.

(12) Allen, F. H.; Kennard, O.; Watson, D. G.; Brammer, L.; Orpen, A. G.; Taylor, R. *J. Chem. Soc., Perkin Trans. 2* **1987**, S1.

(13) Mitzi, D. B. *Prog. Inorg. Chem.* **1999**, *48*, 1.

(14) (a) Ishihara, T.; Takahashi, J.; Goto, T. *Solid State Commun.* **1989**, *69*, 933. (b) Ishihara, T. *J. Lumin.* **1994**, *60−61*, 269.

(15) Muljarov, E. A.; Tikhodeev, S. G.; Gippius, N. A.; Ishihara, T. *Phys. Rev. B: Condens. Matter Mater. Phys.* **1995**, *51*, 14370.

(16) (a) Era, M.; Morimoto, S.; Tsutsui, T.; Saito, S. *Appl. Phys. Lett.* **1994**, *65*, 676. (b) Chondroudis, K.; Mitzi, D. B. *Chem. Mater.* **1999**, *11*, 3028.

(17) Gauthron, K.; Lauret, J. S.; Doyennette, L.; Lanty, G.; Al Choueiry, A.; Zhang, S. J.; Brehier, A.; Largeau, L.; Mauguin, O.; Bloch, J.; et al. *Opt. Express* **2010**, *18*, 5912.

(18) (a) Dohner, E. R.; Hoke, E. T.; Karunadasa, H. I. *J. Am. Chem. Soc.* **2014**, *136*, 1718. (b) Dohner, E. R.; Jaffe, A.; Bradshaw, L. R.; Karunadasa, H. I. *J. Am. Chem. Soc.* **2014**, *136*, 13154.

(19) (a) Calabrese, J.; Jones, N. L.; Harlow, R. L.; Herron, N.; Thorn, D. L.; Wang, Y. *J. Am. Chem. Soc.* **1991**, *113*, 2328. (b) Mitzi, D. B.; Wang, S.; Feild, C. A.; Chess, C. A.; Guloy, A. M. *Science* **1995**, *267*, 1473.

(20) Hong, X.; Ishihara, T.; Nurmikko, A. V. *Phys. Rev. B: Condens. Matter Mater. Phys.* **1992**, *45*, 6961.

(21) Beiley, Z. M.; McGehee, M. D. *Energy Environ. Sci.* **2012**, *5*, 9173.

(22) Cao, D. H.; Stoumpos, C. C.; Farha, O. K.; Hupp, J. T.; Kanatzidis, M. G. *J. Am. Chem. Soc.* **2015**, *137*, 7843.

(23) (a) Yao, K.; Wang, X.; Xu, Y.-x.; Li, F.; Zhou, L. *Chem. Mater.* **2016**, *28*, 3131. (b) Koh, T. M.; Shanmugam, V.; Schlipf, J.; Oesinghaus, L.; Müller-Buschbaum, P.; Ramakrishnan, N.; Swamy, V.; Mathews, N.; Boix, P. P.; Mhaisalkar, S. G. *Adv. Mater.* **2016**, *28*, 3653. (c) Quan, L. N.; Yuan, M.; Comin, R.; Voznyy, O.; Beauregard, E. M.; Hoogland, S.; Buin, A.; Kirmani, A. R.; Zhao, K.; Amassian, A.; et al. *J. Am. Chem. Soc.* **2016**, *138*, 2649.

(24) Kikuchi, K.; Takeoka, Y.; Rikukawa, M.; Sanui, K. *Curr. Appl. Phys.* **2004**, *4*, 599.

(25) Wei, Y.; Audebert, P.; Galmiche, L.; Lauret, J. S.; Deleporte, E. *J. Phys. D: Appl. Phys.* **2013**, *46*, 135105.

(26) Li, X.; Ibrahim Dar, M.; Yi, C.; Luo, J.; Tschumi, M.; Zakeeruddin, S. M.; Nazeeruddin, M. K.; Han, H.; Grätzel, M. *Nat. Chem.* **2015**, *7*, 703.

(27) Jiang, Q.; Rebollar, D.; Gong, J.; Piacentino, E. L.; Zheng, C.; Xu, T. *Angew. Chem., Int. Ed.* **2015**, *54*, 7617.

(28) Daub, M.; Hillebrecht, H. *Angew. Chem., Int. Ed.* **2015**, *54*, 11016.

(29) Ganose, A. M.; Savory, C. N.; Scanlon, D. O. *J. Phys. Chem. Lett.* **2015**, *6*, 4594.

(30) Xiao, Z.; Meng, W.; Saparov, B.; Duan, H.-S.; Wang, C.; Feng, C.; Liao, W.; Ke, W.; Zhao, D.; Wang, J.; et al. *J. Phys. Chem. Lett.* **2016**, *7*, 1213.

(31) Umeyama, D.; Lin, Y.; Karunadasa, H. I. *Chem. Mater.* **2016**, *28*, 3241.

(32) (a) Chen, Y.; Li, B.; Huang, W.; Gao, D.; Liang, Z. *Chem. Commun.* **2015**, *51*, 11997. (b) Halder, A.; Chulliyil, R.; Subbiah, A. S.; Khan, T.; Chattoraj, S.; Chowdhury, A.; Sarkar, S. K. *J. Phys. Chem. Lett.* **2015**, *6*, 3483.

(33) Jaffe, A.; Lin, Y.; Mao, W. L.; Karunadasa, H. I. *J. Am. Chem. Soc.* **2015**, *137*, 1673.

(34) Matsuishi, K.; Suzuki, T.; Onari, S.; Gregoryanz, E.; Hemley, R. J.; Mao, H. K. *Phys. Status Solidi B* **2001**, *223*, 177.

(35) Umebayashi, T.; Asai, K.; Kondo, T.; Nakao, A. *Phys. Rev. B: Condens. Matter Mater. Phys.* **2003**, *67*, 155405.

(36) Vos, A. D. *J. Phys. D: Appl. Phys.* **1980**, *13*, 839.

(37) Suarez, B.; Gonzalez-Pedro, V.; Ripolles, T. S.; Sanchez, R. S.; Otero, L.; Mora-Sero, I. *J. Phys. Chem. Lett.* **2014**, *5*, 1628.

(38) Iwanaga, M.; Hayashi, T. *J. Lumin.* **2003**, *102−103*, 663.

(39) (a) Mizusaki, J.; Arai, K.; Fueki, K. *Solid State Ionics* **1983**, *11*, 203. (b) Kuku, T. A.; Salau, A. M. *Solid State Ionics* **1987**, *25*, 1.

(40) Brivio, F.; Caetano, C.; Walsh, A. *J. Phys. Chem. Lett.* **2016**, *7*, 1083.

(41) Sadhanala, A.; Deschler, F.; Thomas, T. H.; Dutton, S. E.; Goedel, K. C.; Hanusch, F. C.; Lai, M. L.; Steiner, U.; Bein, T.; Docampo, P.; et al. *J. Phys. Chem. Lett.* **2014**, *5*, 2501.

(42) Rehman, W.; Milot, R. L.; Eperon, G. E.; Wehrenfennig, C.; Boland, J. L.; Snaith, H. J.; Johnston, M. B.; Herz, L. M. *Adv. Mater.* **2015**, *27*, 7938.

(43) Beal, R. E.; Slotcavage, D. J.; Leijtens, T.; Bowring, A. R.; Belisle, R. A.; Nguyen, W. H.; Burkhard, G. F.; Hoke, E. T.; McGehee, M. D. *J. Phys. Chem. Lett.* **2016**, *7*, 746.

(44) (a) Hu, M.; Bi, C.; Yuan, Y.; Bai, Y.; Huang, J. *Adv. Sci.* **2016**, *3*, 1500301. (b) Sutter-Fella, C. M.; Li, Y.; Amani, M.; Ager, J. W.; Toma, F. M.; Yablonovitch, E.; Sharp, I. D.; Javey, A. *Nano Lett.* **2016**, *16*, 800.

(45) Shao, Y.; Fang, Y.; Li, T.; Wang, Q.; Dong, Q.; Deng, Y.; Yuan, Y.; Wei, H.; Wang, M.; Gruverman, A.; et al. *Energy Environ. Sci.* **2016**, *9*, 1752.

(46) McMeekin, D. P.; Sadoughi, G.; Rehman, W.; Eperon, G. E.; Saliba, M.; Hörantner, M. T.; Haghighirad, A.; Sakai, N.; Korte, L.; Rech, B.; et al. *Science* **2016**, *351*, 151.

(47) Swainson, I. P.; Tucker, M. G.; Wilson, D. J.; Winkler, B.; Milman, V. *Chem. Mater.* **2007**, *19*, 2401.

(48) (a) Glazer, A. *Acta Crystallogr., Sect. B: Struct. Crystallogr. Cryst. Chem.* **1972**, *28*, 3384. (b) Lufaso, M. W.; Woodward, P. M. *Acta Crystallogr., Sect. B: Struct. Sci.* **2001**, *57*, 725. (c) Here, tilts are described as rotations about the axes of the undistorted cubic unit cell. Letters refer to the relative degree of tilt, where abc or aaa represent three unequal or equal tilts, respectively. A superscript 0 signifies that no tilt occurs along that axis, a superscript + means that all octahedra tilt in the same direction along that axis, and a superscript − means adjacent octahedra along that axis alternate in the tilt direction..

(49) Luty, T.; Eckhardt, C. J. *J. Am. Chem. Soc.* **1995**, *117*, 2441.

(50) Yi, C.; Luo, J.; Meloni, S.; Boziki, A.; Ashari-Astani, N.; Gratzel, C.; Zakeeruddin, S. M.; Rothlisberger, U.; Gratzel, M. *Energy Environ. Sci.* **2016**, *9*, 656.

(51) Conings, B.; Drijkoningen, J.; Gauquelin, N.; Babayigit, A.; D'Haen, J.; D'Olieslaeger, L.; Ethirajan, A.; Verbeeck, J.; Manca, J.; Mosconi, E.; et al. *Adv. Energy Mater.* **2015**, *5*, 1500477.

(52) Eperon, G. E.; Stranks, S. D.; Menelaou, C.; Johnston, M. B.; Herz, L. M.; Snaith, H. J. *Energy Environ. Sci.* **2014**, *7*, 982.

(53) Tosun, B. S.; Hillhouse, H. W. *J. Phys. Chem. Lett.* **2015**, *6*, 2503.

(54) Strevel, N.; Trippel, L.; Gloeckler, M. *Photovoltaics International* **2012**, *17*, 1.

(55) Rodová, M.; Brožek, J.; Knížek, K.; Nitsch, K. *J. Therm. Anal. Calorim.* **2003**, *71*, 667.

(56) Kulbak, M.; Gupta, S.; Kedem, N.; Levine, I.; Bendikov, T.; Hodes, G.; Cahen, D. *J. Phys. Chem. Lett.* **2016**, *7*, 167.

(57) Trots, D. M.; Myagkota, S. V. *J. Phys. Chem. Solids* **2008**, *69*, 2520.

(58) (a) Eperon, G. E.; Paterno, G. M.; Sutton, R. J.; Zampetti, A.; Haghighirad, A. A.; Cacialli, F.; Snaith, H. J. *J. Mater. Chem. A* **2015**, *3*, 19688. (b) Dastidar, S.; Egger, D. A.; Tan, L. Z.; Cromer, S. B.; Dillon, A. D.; Liu, S.; Kronik, L.; Rappe, A. M.; Fafarman, A. T. *Nano Lett.* **2016**, *16*, 3563.

(59) Needleman, H. *Annu. Rev. Med.* **2004**, *55*, 209.

(60) Hsu, P.-C.; Guo, Y. L. *Toxicology* **2002**, *180*, 33.

(61) Bressler, J.; Kim, K.-a.; Chakraborti, T.; Goldstein, G. *Neurochem. Res.* **1999**, *24*, 595.

(62) Babayigit, A.; Ethirajan, A.; Muller, M.; Conings, B. *Nat. Mater.* **2016**, *15*, 247.

(63) Clever, H. L.; Johnston, F. J. *J. Phys. Chem. Ref. Data* **1980**, *9*, 751.

(64) Scaife, D. E.; Weller, P. F.; Fisher, W. G. *J. Solid State Chem.* **1974**, *9*, 308.

(65) Thiele, G.; Rotter, H. W.; Schmidt, K. D. *Z. Anorg. Allg. Chem.* **1987**, *545*, 148.

(66) (a) Hao, F.; Stoumpos, C. C.; Cao, D. H.; Chang, R. P. H.; Kanatzidis, M. G. *Nat. Photonics* **2014**, *8*, 489. (b) Noel, N. K.; Stranks, S. D.; Abate, A.; Wehrenfennig, C.; Guarnera, S.; Haghighirad, A. A.; Sadhanala, A.; Eperon, G. E.; Pathak, S. K.; Johnston, M. B.; et al. *Energy Environ. Sci.* **2014**, *7*, 3061.

(67) Norrby, L. J. *J. Chem. Educ.* **1991**, *68*, 110.

(68) Mohan, R. *Nat. Chem.* **2010**, *2*, 336.

(69) (a) Zhao, K.; Zhang, X.; Zhang, L. *Electrochem. Commun.* **2009**, *11*, 612. (b) Ahmmad, B.; Kurawaki, J.; Ohkubo, T.; Hirose, F. *J. Energy Eng.* **2013**, *139*, 338.

(70) (a) Hahn, N. T.; Self, J. L.; Mullins, C. B. *J. Phys. Chem. Lett.* **2012**, *3*, 1571. (b) Hahn, N. T.; Rettie, A. J. E.; Beal, S. K.; Fullon, R. R.; Mullins, C. B. *J. Phys. Chem. C* **2012**, *116*, 24878.

(71) (a) Lindqvist, O.; Johansson, G.; Sandberg, F.; Norin, T. *Acta Chem. Scand.* **1968**, *22*, 2943. (b) Jakubas, R.; Zaleski, J.; Sobczyk, L. *Ferroelectrics* **1990**, *108*, 109.

(72) (a) Lehner, A. J.; Fabini, D. H.; Evans, H. A.; Hébert, C.-A.; Smock, S. R.; Hu, J.; Wang, H.; Zwanziger, J. W.; Chabinyc, M. L.; Seshadri, R. *Chem. Mater.* **2015**, *27*, 7137. (b) Park, B.-W.; Philippe, B.; Zhang, X.; Rensmo, H.; Boschloo, G.; Johansson, E. M. J. *Adv. Mater.* **2015**, *27*, 6806. (c) Hoye, R. L. Z.; Brandt, R. E.; Osherov, A.; Stevanović, V.; Stranks, S. D.; Wilson, M. W. B.; Kim, H.; Akey, A. J.; Perkins, J. D.; Kurchin, R. C.; et al. *Chem. - Eur. J.* **2016**, *22*, 2605.

(73) Saparov, B.; Hong, F.; Sun, J.-P.; Duan, H.-S.; Meng, W.; Cameron, S.; Hill, I. G.; Yan, Y.; Mitzi, D. B. *Chem. Mater.* **2015**, *27*, 5622.

(74) (a) Lehner, A. J.; Wang, H.; Fabini, D. H.; Liman, C. D.; Hébert, C.-A.; Perry, E. E.; Wang, M.; Bazan, G. C.; Chabinyc, M. L.; Seshadri, R. *Appl. Phys. Lett.* **2015**, *107*, 131109. (b) Brandt, R. E.; Kurchin, R. C.; Hoye, R. L. Z.; Poindexter, J. R.; Wilson, M. W. B.; Sulekar, S.; Lenahan, F.; Yen, P. X. T.; Stevanović, V.; Nino, J. C.; et al. *J. Phys. Chem. Lett.* **2015**, *6*, 4297.

(75) Cortecchia, D.; Dewi, H. A.; Yin, J.; Bruno, A.; Chen, S.; Baikie, T.; Boix, P. P.; Grätzel, M.; Mhaisalkar, S.; Soci, C.; et al. *Inorg. Chem.* **2016**, *55*, 1044.

(76) Shinada, M.; Sugano, S. *J. Phys. Soc. Jpn.* **1966**, *21*, 1936.

(77) Gregg, B. A. *J. Phys. Chem. B* **2003**, *107*, 4688.

(78) (a) Yin, W.-J.; Yang, J.-H.; Kang, J.; Yan, Y.; Wei, S.-H. *J. Mater. Chem. A* **2015**, *3*, 8926. (b) Du, M. H. *J. Mater. Chem. A* **2014**, *2*, 9091. (c) Brandt, R. E.; Stevanović, V.; Ginley, D. S.; Buonassisi, T. *MRS Commun.* **2015**, *5*, 265.

(79) Vasala, S.; Karppinen, M. *Prog. Solid State Chem.* **2015**, *43*, 1.

(80) Werker, W. *Recl. Trav. Chim. Pays-Bas* **1939**, *58*, 257.

(81) Saparov, B.; Sun, J.-P.; Meng, W.; Xiao, Z.; Duan, H.-S.; Gunawan, O.; Shin, D.; Hill, I. G.; Yan, Y.; Mitzi, D. B. *Chem. Mater.* **2016**, *28*, 2315.

(82) Lee, B.; Stoumpos, C. C.; Zhou, N.; Hao, F.; Malliakas, C.; Yeh, C.-Y.; Marks, T. J.; Kanatzidis, M. G.; Chang, R. P. H. *J. Am. Chem. Soc.* **2014**, *136*, 15379.

(83) Meyer, G. *Prog. Solid State Chem.* **1982**, *14*, 141.

(84) Morss, L. R.; Siegal, M.; Stenger, L.; Edelstein, N. *Inorg. Chem.* **1970**, *9*, 1771.

(85) Kojima, N. *Bull. Chem. Soc. Jpn.* **2000**, *73*, 1445.

(86) Elliott, N.; Pauling, L. *J. Am. Chem. Soc.* **1938**, *60*, 1846.

(87) Retuerto, M.; Emge, T.; Hadermann, J.; Stephens, P. W.; Li, M. R.; Yin, Z. P.; Croft, M.; Ignatov, A.; Zhang, S. J.; Yuan, Z.; et al. *Chem. Mater.* **2013**, *25*, 4071.

(88) (a) Smit, W. M. A.; Dirksen, G. J.; Stufkens, D. J. *J. Phys. Chem. Solids* **1990**, *51*, 189. (b) Morrs, L. R.; Robinson, W. R. *Acta Crystallogr., Sect. B: Struct. Crystallogr. Cryst. Chem.* **1972**, *28*, 653. (c) Prokert, F.; Aleksandrov, K. S. *Phys. Status Solidi B* **1984**, *124*, 503.

(89) Beznosikov, B. V.; Mosyul, S. V. *Sov. Phys. Crystallogr.* **1978**, *23*, 622.

(90) McClure, E. T.; Ball, M. R.; Windl, W.; Woodward, P. M. *Chem. Mater.* **2016**, *28*, 1348.

(91) Volonakis, G.; Filip, M. R.; Haghighirad, A. A.; Sakai, N.; Wenger, B.; Snaith, H. J.; Giustino, F. *J. Phys. Chem. Lett.* **2016**, *7*, 1254.

(92) Wei, F.; Deng, Z.; Sun, S.; Xie, F.; Kieslich, G.; Evans, D. M.; Carpenter, M. A.; Bristowe, P. D.; Cheetham, A. K. *Mater. Horiz.* **2016**, *3*, 328.

(93) Cuevas, A.; Macdonald, D. *Sol. Energy* **2004**, *76*, 255.

(94) Gurney, R. W.; Mott, N. F. *Proc. R. Soc. London, Ser. A* **1938**, *164*, 151.

(95) (a) Niu, G.; Guo, X.; Wang, L. *J. Mater. Chem. A* **2015**, *3*, 8970. (b) Leijtens, T.; Eperon, G. E.; Noel, N. K.; Habisreutinger, S. N.; Petrozza, A.; Snaith, H. J. *Adv. Energy Mater.* **2015**, *5*, 1500963.

(96) Unger, E. L.; Hoke, E. T.; Bailie, C. D.; Nguyen, W. H.; Bowring, A. R.; Heumuller, T.; Christoforo, M. G.; McGehee, M. D. *Energy Environ. Sci.* **2014**, *7*, 3690.